LANGMUIR

pubs.acs.org/Langmuir Article

A Hole-Selective Self-Assembled Monolayer for Both Efficient Perovskite and Organic Solar Cells

Mingliang Li, Zhenzhu Li, Ming Liu, Huiting Fu, Feng Qi, Francis R. Lin, Aron Walsh,* and Alex K.-Y. Jen*

Cite This: *Langmuir* 2024, 40, 4772–4778 Read Online

ACCESS | Metrics & More | Article Recommendations | Supporting Information

ABSTRACT: Self-assembled monolayers (SAMs) emerging as promising hole-selective layers (HSLs) are advantageous for facile processability, low cost, and minimal material consumption in the fabrication of both perovskite solar cells (PSCs) and organic solar cells (OSCs). However, owing to the different nature between perovskites and organic semiconductors, few SAMs were reported to effectively accommodate both PSCs and OSCs at the same time. In this regard, a universally applicable SAM that can accommodate both perovskites and organic semiconductors could be desirable for simplifying cell manufacturing, especially from an industrial perspective. In this work, we designed a SAM, **TDPA-Cl** by introducing chlorinated phenothiazine as the headgroup and linking with anchor phosphonic acid through a butyl chain. The resulting dense SAM was carefully characterized in terms of molecular bonding, surface morphology, and packing density, and its functions in OSCs and PSCs were discussed from the aspects of interactions with the absorber layer, energy level alignment, and charge-selective dipoles. The PM6:Y6-based OSCs with **TDPA-Cl** SAM as the HSL showed a superior performance to those with PEDOT:PSS. Furthermore, the universality was proved with an efficiency of 17.4% in the D18:Y6 system. In PSCs, the **TDPA-Cl**-based devices delivered a better performance of 22.4% than the PTAA-based devices (20.8%) with improved processability and reproducibility. This work represents a SAM with reasonably good compromise between the differing requirements of OSCs and PSCs.

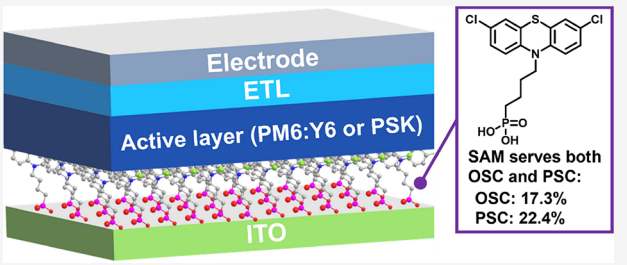

INTRODUCTION

Recently, inverted (p-i-n) perovskite solar cells (PSCs) have received great attention[1−5] due to their low-temperature processability and better compatibility with flexible substrates[6,7] and tandem device fabrication.[8−10] However, both the lower power conversion efficiency (PCE) than conventional (n-i-p) PSCs, and potential stability problems, limited their further improvement and applications. One of the reasons stems from the traps located at the interface between perovskite and hole-selective layers (HSLs), resulting in severe charge recombination and poor charge extraction.[11] Among the commercial HSLs, poly[bis(4-phenyl)(2,4,6-trimethylphenyl]amine (PTAA) has always been criticized for energy level mismatch and wetting problems.[12,13] Coincidently, p-i-n organic solar cells (OSCs) face the similar dilemma, where corrosivity, hygroscopicity, high cost, and parasitic absorption of the traditional HSL poly(3,4-ethylenedioxythiophene):poly(styrenesulfonate) (PEDOT:PSS) limit the device performance and compromise the long-term stability.[14−16] On this basis, some small organic molecules derived from conventional HSLs were developed and solved some problems, but new materials with good film stability and strong interaction or adhesion with the adjacent layers are still needed.[17−19]

Compared with the above-mentioned materials, self-assembled monolayers (SAMs) emerge as new candidates for HSLs in photovoltaic devices and offer great potential in industrial manufacturing due to their compatibility with diverse substrates, easier dopant-free processing procedures, minimum material consumption, low cost, and green-solvent processability.[20−22] Structures of SAMs can be easily modified to fit different PSC and OSC systems. For example, Hong et al. selected bromine-substituted phenothiazine as the SAM backbone, acting as the HSL in PSCs for the first time. As a result, a PCE up to 22.44% can be obtained with a high open-circuit voltage (V_{OC}) of 1.09 V and fill factor (*FF*) of 81%, owing to the well-matched energy level and efficient trap passivation at the interface.[12] Albrecht and co-workers investigated the performance of the PSCs with different carbazole-based SAMs and further fabricated a monolithic perovskite/silicon tandem cell with a certified PCE of 29.15%.[9]

Received: November 23, 2023
Revised: February 9, 2024
Accepted: February 9, 2024
Published: February 21, 2024

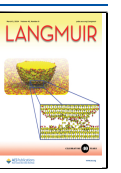

Downloaded via Aron Walsh on March 30, 2024 at 09:25:17 (UTC).
See https://pubs.acs.org/sharingguidelines for options on how to legitimately share published articles.

ACS Publications © 2024 American Chemical Society

In OSCs, Anthopoulos et al. obtained a maximum PCE of 18.03% with the 2PACz SAM as the HSL in the PM6:BTPeC9:$PC_{71}BM$ bulk-heterojunction (BHJ) cell, where the superior performance can be attributed to lower contact resistance, reduced recombination losses, and improved interfacial charge transport.[23] To further explore the effect of SAM conformations, Janssen et al. designed carbazole-based SAMs with different alkyl chains, and a high PCE of 17.4% was realized in the OSC based on PM6:BTPeC9 with 3PACz SAM.[14]

Although SAM-based photovoltaic devices are well developed (Tables S1 and S2), OSCs and PSCs generally require different SAMs with variant film qualities owing to their different intrinsic natures, which could complicate SAM processing technologies and potentially increase the cost for SAM industrialization. To address these issues, we designed and synthesized a versatile SAM molecule named **TDPA-Cl**. The chlorinated phenothiazine was selected as the headgroup and was linked to anchor phosphonic acid through a butyl chain. The SAM was spin-coated on the ITO substrate, followed by thorough characterization and investigation of SAM qualities and functions in OSCs and PSCs.

Compared with the commonly used PTAA in PSCs, the **TDPA-Cl** SAM showed a higher PCE of 22.4% with enhanced processability and device reproducibility. Moreover, in OSCs based on PM6:Y6, the **TDPA-Cl** SAM showed a device performance superior to that of devices with PEDOT:PSS, and its universality was also proved with the D18:Y6 system with a PCE of 17.4%. As a result, **TDPA-Cl** was demonstrated as a potential candidate in replacing PTAA and PEDOT:PSS for HSLs. Our work represents a reasonably good compromise between the differing requirements of OSCs and PSCs and provides insights into new SAM development in photovoltaic devices.

RESULTS AND DISCUSSIONS

TDPA-Cl is designed to fit in both OSCs and PSCs (Figure 1), so the intrinsic characteristics of the organic semiconductor

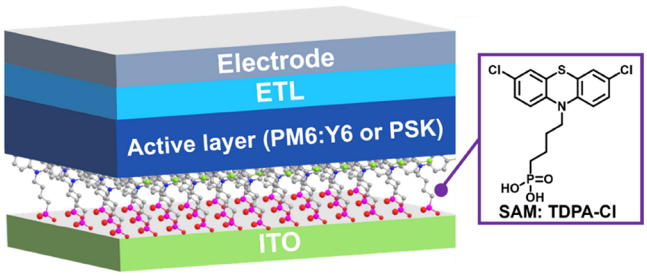

Figure 1. Schematic cross-section of the solar cell with **TDPA-Cl** SAM as the HSL. The active layers are PM6:Y6 or perovskite (labeled as PSK). The inset shows the chemical structure of **TDPA-Cl**. ETL: electron transport layer; PSK: perovskite.

and perovskite should be carefully considered. Due to the limited exciton dissociation efficiency in OSCs compared to PSCs, **TDPA-Cl** was designed with the electron-rich phenothiazine scaffold instead of conventional carbazole to facilitate the charge carrier transport and extraction in both OSCs and PSCs. Compared with the brominated-phenothiazine, the chlorine substituents can mildly downshift the molecular energy level for the energy alignment and tune the dipole for the charge selection in both OSCs and PSCs,[37] as well as achieve denser and more regular packing due to the size effect of smaller chlorine atoms.[24] Besides, the halogen and sulfur heteroatoms can further enhance the PSC device performance by interfacial passivation.[25−28] Phosphonic acid was selected as the anchor group to passivate the defects on the metal oxide substrate via covalent bonds.[29] An *n*-butyl chain connecting the phenothiazine headgroup and phosphonic acid anchor could modulate the material flexibility and interaction between the functional head and the substrate for dense packing with optimized conformation.[30,31]

A densely packed SAM with minimal defects is crucial for functioning as an efficient HSL in highly efficient and stable solar cells. The as-prepared SAM was characterized to reveal their molecular bonding, surface morphology, and packing density on the substrate surface.

Interface defects can be eliminated by chemical bonding between anchors and the substrate, which could be evidenced by characteristic peaks at 1264 (stretching vibrations of C−N) and 1459 cm^{-1} (phenothiazine ring stretching vibrations) in the attenuated total reflection-Fourier transform infrared spectroscopy (ATR-FTIR, Figure 2a),[32,33] and the signals of the molecular characteristic elements, including Cl, N, P, and S,[34,35] in X-ray photoelectron spectroscopy (XPS, Figures 2b, S1, and S2) measurements. The covalent bonding could be further identified for the fitted fingerprint peaks at 533.0 eV assigned to In−O−P/P═O, while the other two fitted peaks at 532.1 and 531.4 eV were originated from the ITO substrate (Figure 2c).[12,23,29]

To further investigate the morphology of SAM-decorated ITO, atomic force microscopy (AFM) and scanning electron microscopy (SEM) techniques were performed. In the AFM images, **TDPA-Cl**-decorated ITO showed a comparable roughness (1.19 nm, Figure 2d) to that of a clean ITO (1.10 nm, Figure S3) because of having an ultrathin SAM coverage. With the energy dispersive spectroscopy (EDS) modules of SEM, the characteristic elements of Cl, N, P, and S of **TDPA-Cl** showed a uniform distribution on the substrate, indicating no severe aggregations formed on the SAM-decorated ITO surface (Figures 2e, S5, and S6).[36]

The molecular SAM density was calculated as 4.6×10^{-10} mol cm^{-2} by a UV−vis-based method[37] from Figures 2f and S7 and delivered areas per molecule (S) of 33.0 $Å^2$, which is within a similar range with some other reported SAMs (~20 $Å^2$).[38,39] The packing quality was further investigated with the time-dependent contact angle measurements in Figure 2g and Table S3. As small-sized water molecules will gradually permeate through the SAM to the hydrophilic anchor and substrate, leading to the decreased contact angle with time, a big decay constant k of 2.24 min^{-1} and contact angle of 18.8° after 10 min indicate the dense and regular packing of the SAMs.[40,41]

The functions of the **TDPA-Cl** SAM in OSCs and PSCs can be discussed from the aspects of interactions with adjacent layers, energy level alignment, and charge-selective dipoles. Theoretical calculations were conducted to simulate the SAM interfacial interaction (Figure 3a) and molecular dynamic distribution (Figure 3b) in PSCs.[37] As we expected, orbital overlaps were found between PbI_2-terminated perovskite[43] and **TDPA-Cl** SAMs with a binding energy of −0.235 eV/molecule, which indicate that **TDPA-Cl** SAM plays an active role in the formation of the high-quality perovskite film mainly due to the Lewis acid−base interaction between heteroatom (S and Cl) and Pb^{2+}.[44] In OSCs, the interface compatibility is also

https://doi.org/10.1021/acs.langmuir.3c03610
Langmuir 2024, 40, 4772−4778

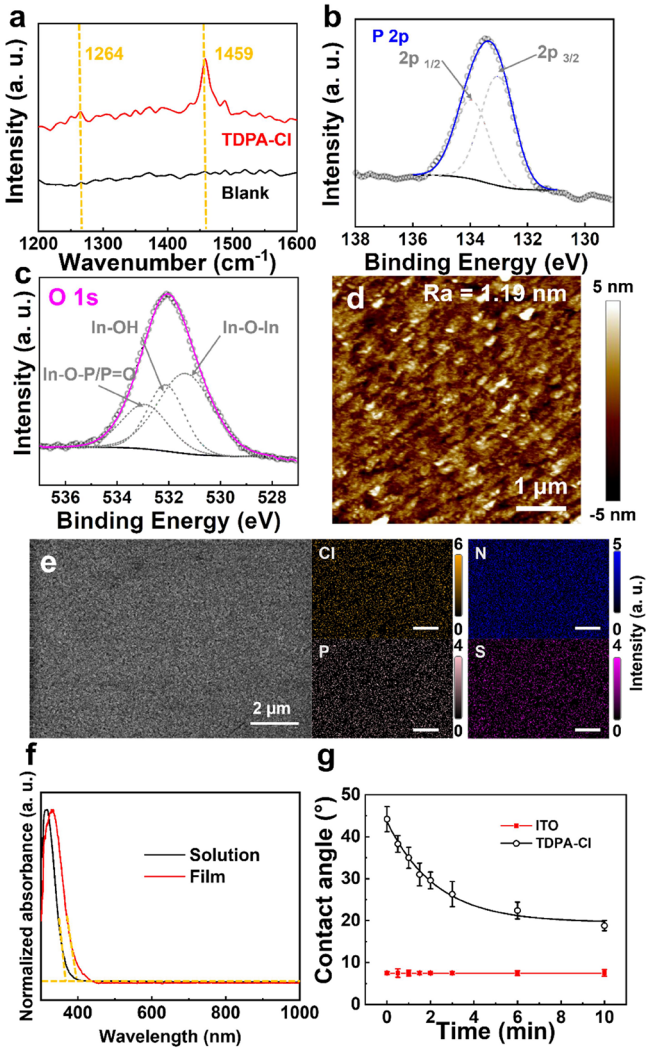

Figure 2. Characterization of the **TDPA-Cl** SAM. (a) ATR-FTIR absorbance spectra of the **TDPA-Cl** SAM on ITO. (b,c) High-resolution XPS of P 2p and O 1s with the **TDPA-Cl** SAM, respectively. The P 2p peak centered at 133.4 eV consists of the two components: 132.9 eV (P 2P $_{3/2}$) and 133.8 eV (P 2P $_{1/2}$).[42] (d) AFM image of the **TDPA-Cl** SAM on ITO. (e) SEM image and its corresponding Cl (orange), N (blue), P (pink), and I (purple) element EDS mapping of the **TDPA-Cl** SAM on ITO. (f) Normalized UV−vis spectra of **TDPA-Cl** in solutions (10^{-5} M) and solid films. (g) Time-dependent contact-angle measurements.

significantly improved due to the aromatic nature of **TDPA-Cl** as evidenced by the contact angle measurements of Figure 2g.[23]

The energy levels of the **TDPA-Cl** SAM were determined by cyclic voltammetry (CV) and UV−vis measurements (Figures S7 and S8). The highest occupied molecular orbital (HOMO) and the lowest unoccupied molecular orbital (LUMO) energy levels were calculated to be −5.42 and −2.30 eV, respectively, which were consistent with the HOMO of 5.47 eV from ultraviolet photoelectron spectroscopy (UPS) (Figures 3c, S10, and S16). Therefore, the **TDPA-Cl** SAM showed a good energy level alignment with both perovskite (valence band maximum, VBM: −5.90 eV) in PSCs[29] and PM6 (HOMO: −5.56 eV) in OSCs[45], which could facilitate the efficient hole extraction and electron blocking toward the anode.

The dipole of **TDPA-Cl** was calculated as 3.81 D pointing downward the substrate by DFT calculations (Figure 3d), which will help downshift the ITO work function[29,46] and facilitate charge selection through forming an interfacial electric field.[47] As the shown in UPS measurements (Figures 3c and S9), the work function of the **TDPA-Cl**-decorated ITO is 5.00 eV, deeper than those of PTAA and PEDOT:PSS, which is favorable for efficient hole-extraction at the interface by minimizing the energy offset to achieve higher *FF* and V_{OC} of the corresponding photovoltaic devices.[12,29]

Photovoltaic performance based on **TDPA-Cl** SAM was further characterized. Figure 4a,b shows the representative current density−voltage (J−V) curves and EQE plots. Table 1 summarizes the related photovoltaic parameters of derived OSCs and PSCs. First, the conventional device structure of ITO/SAM/PM6:Y6/PNDIT-F3N/Ag was adopted in the OSCs. Compared with the PCE of 16.6% from PEDOT:PSS, the **TDPA-Cl**-based device exhibited an enhanced PCE of 17.3% with an *FF* of 75.7%, V_{oc} of 0.860 V, and J_{sc} of 26.6 mA·cm^{-2} under 1 sun illumination (AM 1.5G, 100 mW·cm^{-2}). In addition, the **TDPA-Cl** SAM showed a good universality when applied to a different active material system of D18:Y6, delivering a high PCE of 17.4% with an *FF* of 75.6%, V_{oc} of 0.832 V, and J_{sc} of 27.6 mA·cm^{-2} (Figure S11). It is notable that the OSC performance enhancement can be mainly attributed to the distinct *FF* values induced by the better energy level alignment and interfacial conditions.[37] Moreover, the PSCs employing **TDPA-Cl** SAM showed a PCE of 22.4%, *FF* of 81.4%, V_{oc} of 1.151 V, and J_{sc} of 23.9 mA·cm^{-2} in a device with a configuration of ITO/SAM/perovskite/C_{60}/BCP/Ag, which was superior to that of PTAA with a PCE of 20.8%. The designed Cl and S effectively passivated the perovskite surface,[12,48,49] improving the *FF* and V_{oc} in the PSCs and further enhancing the PCE. The material stability and SAM-based device stability are revealed in Figures S4, S12, S13, and S14. Although there is still a gap between **TDPA-Cl**- and carbazole-based SAMs in device performance, **TDPA-Cl** demonstrates optimized performance in both OSCs and PSCs compared with traditional HSLs. The universality can be attributed to the structural design of **TDPA-Cl** in the three aspects we mentioned: energy level, molecular dipole, and interaction with adjacent layers.

Compared with carbazole, phenothiazine is an electron-rich scaffold with good chemical stability and very high hole mobilities, which can facilitate exciton dissociation efficiency in OSCs.[12] Chlorine as an electron-withdrawing heteroatom can appropriately adjust the molecular energy level and dipole for good energy alignment and effective charge selection in both the OSCs and PSCs. On the contrary, carbazole-based molecules are predominantly used in high-performance PSCs benefiting from their matching energy levels with perovskite (VBM: −5.90 eV).[9,20,29] However, their deeper energy levels make it challenging to accommodate organic semiconductors (e.g., PM6 HOMO: −5.56 eV)[45] at the same time.

On the other hand, both phenothiazine- and carbazole-based SAMs can exhibit good wettability to organic semiconductors in OSCs due to their organic nature. In PSCs, though with high performance, a carbazole-based SAM still suffers from poor wettability. On this basis, chlorinated phenothiazine with electron-donating atoms (sulfur and chlorine) in top exposed positions can effectively improve the wettability and device performance by strengthened interaction with the perovskite.

https://doi.org/10.1021/acs.langmuir.3c03610
Langmuir 2024, 40, 4772−4778

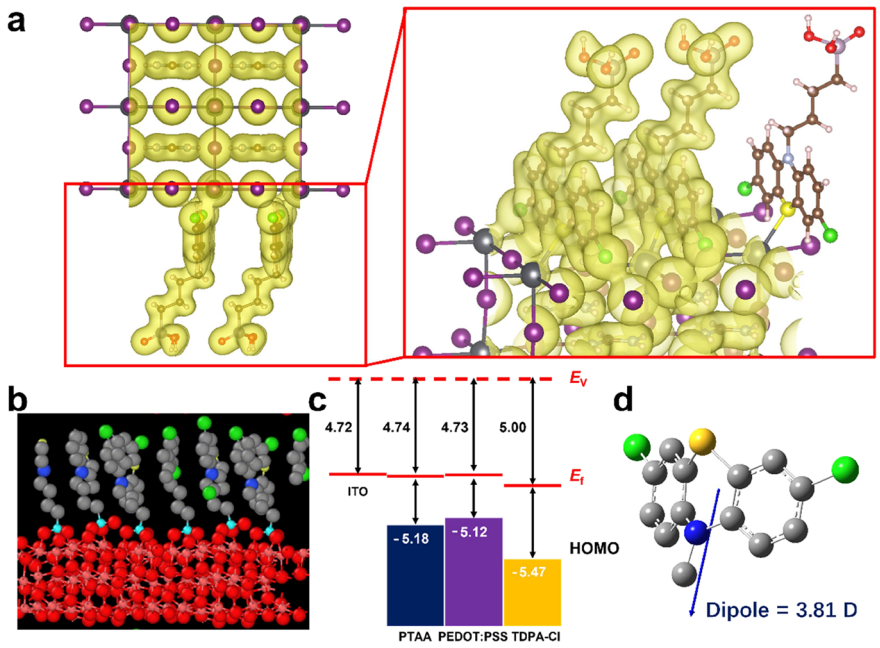

Figure 3. (a) Interfacial orbital distribution of **TDPA-Cl** and perovskite from the DFT calculation. The inset shows the orbital overlap between **TDPA-Cl** and perovskite. (b) MD calculations of **TDPA-Cl** molecules on ITO at the concentration of 3 molecules/15 Å^2. The hydrogen atoms are omitted. (c) Energy level diagram of PTAA, PEDOT:PSS, and **TDPA-Cl** from UPS. E_v and E_f are the vacuum energy level and Fermi level, respectively. (d) Image for the dipole of **TDPA-Cl**. The dipole is from the positive to negative centers. To simplify the calculation, the alkyl chains and phosphonic acid are omitted with methyl groups.

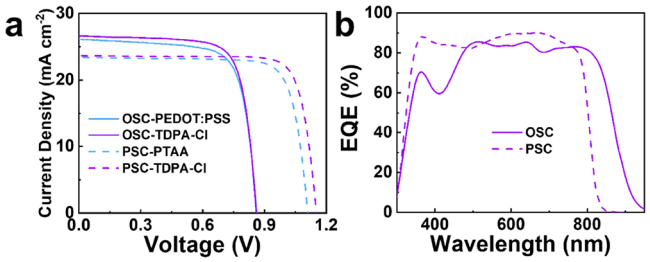

Figure 4. Performances of the photovoltaic devices with the **TDPA-Cl** SAM as the HSL. (a) J–V curves. (b) EQE curves.

Table 1. Performance Table for OSC (PM6:Y6) and PSC

	HTL	V_{oc} (V)	J_{sc} (mA/cm^2)	PCE (%)	FF (%)
OPV	PEDOT:PSS	0.863	26.1	16.6	73.8
	TDPA-Cl	0.860	26.6	17.3	75.7
PSC	PTAA	1.109	24.0	20.8	79.7
	TDPA-Cl	1.151	23.9	22.4	81.4

CONCLUSIONS

In conclusion, we designed and explored a chlorinated phenothiazine-based SAM (**TDPA-Cl**) as an effective HSLs in both OSCs and PSCs. A dense SAM with good regularity was fabricated by spin-coating and the quality of interfaces in both PSCs and OSCs was significantly improved, evidenced by SAM characterization and photovoltaic device applications. The **TDPA-Cl** SAM showed a superior performance than PEDOT:PSS in the PM6:Y6-based OSCs, and its universality was also proved with the D18:Y6 system, resulting in a PCE of 17.4%. In PSCs, the **TDPA-Cl** SAM improved the device performance to 22.4%, which was higher than 20.8% of PTAA-based devices. The performance of the **TDPA-Cl** SAM showed great potential in replacing conventional HSLs. This work provides insight for designing new SAMs compatible with different photovoltaic applications.

EXPERIMENTAL SECTION

UV–Vis Absorption. UV–vis absorption measurements of solution and thin films were determined with an Agilent Cary 8454 spectrophotometer. All film samples were spin-cast on the indium tin oxide (ITO) substrates. Solution UV–vis aborption spectra were collected from the isopropanol solution with the concentration of 1.0 × 10^{-5} M. The SAM surface coverage, Γ (mol cm^{-2}) was quantified in eq S1:

$$\Gamma = \frac{A(\lambda)/\varepsilon(\lambda)}{1000} \quad \text{(S1)}$$

$A(\lambda)$ is the UV–vis absorbance of SAM in Figure S7, and $\varepsilon(\lambda)$ is the molar extinction coefficient of the SAM in solution calculated from the absorbance maximum at ca. 319 nm. In this work, $\varepsilon(\lambda)$ and Γ were calculated as 3.82 × 10^4 M^{-1} cm^{-1} and 2.93 × 10^{-9} mol cm^{-2}, respectively.

Cyclic Voltammetry. CV measurements were conducted by a CHI660D electrochemical workstation in acetonitrile containing Tetrabutylammonium phosphorus hexafluoride (Bu_4NPF_6, 0.1 M) as a supporting electrolyte. A glassy carbon electrode was used as a working electrode, and a platinum wire was used as a counter electrode. All potentials were recorded versus Ag/AgCl as the reference electrode. Before measurements, the solution was deoxygenated by nitrogen bubbling for 10 min. The energy levels of organic semiconductors were calculated using the ferrocene value of −4.8 eV as the reference. The scan rate was 50 mV s^{-1}. The film samples were prepared by dropping the solution (1 mg mL^{-1}) onto the glassy carbon electrodes overnight.

X-ray Photoelectron Spectroscopy. XPS data were obtained with an Axis Ultra Imaging X-ray Photoelectron Spectrometer from Kratos Analytical Ltd. by using 300 W AlKα radiation. The base pressure was about 3 × 10^{-9} mbar. The binding energies were referenced to the C 1s line at 284.8 eV from adventitious carbon.

Ultraviolet Photoelectron Spectroscopy. UPS is conducted in a surface analysis system (VG ESCALAB 220i-XL) equipped with a

https://doi.org/10.1021/acs.langmuir.3c03610
Langmuir 2024, 40, 4772−4778

He discharge lamp ($h\nu$ = 21.22 eV). The samples are deposited on ITO in the same process as for device fabrication. The binding energies were referenced to the Ag signal.

Contact Angle. Contact angle is measured with a DataPhysics contact angle tester 3/13, and the water drop volume is 0.4 mL.

Time-dependent contact angle tests can be exponentially fitted with the following equation:

$$y = y_o + A\exp(-x/k) \quad \text{(S2)}$$

where y_0 and A are fitting constants. k is the decay constant. Herein, the fitting index, R^2 = 0.99168.

Scanning Electron Microscope (SEM) and Energy-Dispersive X-ray Spectroscopy (EDS). The SEM images and EDS mappings were obtained with Hitachi Regulus 8220 ultrahigh-resolution SEM and Octane Elect America EDAX. The scan voltage is 1.0 kV

Thermogravimetric Analysis (TGA). TGA measurements were conducted on a TA Instruments Q600 SDT thermal analysis system under N_2 at a heating rate of 10 °C min^{-1}.

Differential Scanning Calorimetry (DSC). DSC measurements were conducted by using a TA Instruments Q2000 differential scanning calorimeter under N_2.

Attenuated Total Reflection-Fourier Transform Infrared Spectroscopy. The ATR-FTIR spectrum was obtained using a Bruker Tensor 27 FTIR spectrometer. A spectrum was obtained by subtracting the ITO background signal from the signal of the SAM-modified ITO substrate.

Atomic Force Microscopy. The morphology of thin films was investigated by a ScanAsyst model AFM (Bruker Dimension Icon with Nanoscope V controller) under ambient conditions. The resolution of the AFM image is 512 × 512 pixels.

■ ASSOCIATED CONTENT

Supporting Information

The Supporting Information is available free of charge at https://pubs.acs.org/doi/10.1021/acs.langmuir.3c03610.

General methods and supplementary data for molecular synthesis, material characterization, and device investigation (PDF)

■ AUTHOR INFORMATION

Corresponding Authors

Aron Walsh − *Department of Materials, Imperial College London, Exhibition Road, London SW7 2AZ, United Kingdom; Department of Physics, EWHA Womans University, Seoul 03760, South Korea;* orcid.org/0000-0001-5460-7033; Email: a.walsh@imperial.ac.uk

Alex K.-Y. Jen − *Department of Materials Science and Engineering, City University of Hong Kong, Kowloon 999077, Hong Kong; Department of Chemistry and Hong Kong Institute for Clean Energy, City University of Hong Kong, Kowloon 999077, Hong Kong; State Key Laboratory of Marine Pollution, City University of Hong Kong, Hong Kong 999077, China;* orcid.org/0000-0002-9219-7749; Email: alexjen@cityu.edu.hk

Authors

Mingliang Li − *Department of Materials Science and Engineering, City University of Hong Kong, Kowloon 999077, Hong Kong; Hong Kong Institute for Clean Energy, City University of Hong Kong, Kowloon 999077, Hong Kong; State Key Laboratory of Marine Pollution, City University of Hong Kong, Hong Kong 999077, China;* orcid.org/0000-0002-6181-5954

Zhenzhu Li − *Department of Materials, Imperial College London, Exhibition Road, London SW7 2AZ, United Kingdom; Department of Physics, EWHA Womans University, Seoul 03760, South Korea;* orcid.org/0000-0002-6669-563X

Ming Liu − *Department of Materials Science and Engineering, City University of Hong Kong, Kowloon 999077, Hong Kong; Hong Kong Institute for Clean Energy, City University of Hong Kong, Kowloon 999077, Hong Kong; State Key Laboratory of Marine Pollution, City University of Hong Kong, Hong Kong 999077, China*

Huiting Fu − *Department of Materials Science and Engineering, City University of Hong Kong, Kowloon 999077, Hong Kong; Hong Kong Institute for Clean Energy, City University of Hong Kong, Kowloon 999077, Hong Kong; State Key Laboratory of Marine Pollution, City University of Hong Kong, Hong Kong 999077, China*

Feng Qi − *Department of Chemistry and Hong Kong Institute for Clean Energy, City University of Hong Kong, Kowloon 999077, Hong Kong; State Key Laboratory of Marine Pollution, City University of Hong Kong, Hong Kong 999077, China;* orcid.org/0000-0003-3814-3317

Francis R. Lin − *Department of Chemistry and Hong Kong Institute for Clean Energy, City University of Hong Kong, Kowloon 999077, Hong Kong; State Key Laboratory of Marine Pollution, City University of Hong Kong, Hong Kong 999077, China;* orcid.org/0000-0002-4651-9145

Complete contact information is available at: https://pubs.acs.org/10.1021/acs.langmuir.3c03610

Author Contributions

Z.L. and A.W. performed the theoretical calculation. M.L. and H.F. fabricated and tested the PSCs and OSCs, respectively. F.Q. participated in the discussion. M.L. conducted the rest of the experiments. A.K.-Y.J., F.R.L., and M.L. raised this project and wrote the paper. The manuscript was written through contributions of all authors. All authors have given approval to the final version of the manuscript. M.L. and Z.L. contributed equally.

Funding

A.K.-Y.J. thanks the sponsorship of the Lee Shau-Kee Chair Professor (Materials Science), and the support from the APRC Grant of the City University of Hong Kong (9380086, 9610508), the TCFS Grant (GHP/018/20SZ) and MRP Grant (MRP/040/21X) from the Innovation and Technology Commission of Hong Kong, the Green Tech Fund (202020164) from the Environment and Ecology Bureau of Hong Kong, the GRF grants (11307621, 11316422) from the Research Grants Council of Hong Kong, Shenzhen Science and Technology Program (SGDX20201103095412040), Guangdong Major Project of Basic and Applied Basic Research (2019B030302007), Guangdong-Hong Kong-Macao Joint Laboratory of Optoelectronic and Magnetic Functional Materials (2019B121205002), the US Office of Naval Research (N00014-20-1-2191), and the CRF grant (C6023-19GF) from the Research Grants Council of Hong Kong.

Notes

The authors declare no competing financial interest.

■ ABBREVIATIONS

SAMs, self-assembled monolayers; HSLs, hole-selective layers; PSCs, perovskite solar cells; OSCs, organic solar cells; PCE,

https://doi.org/10.1021/acs.langmuir.3c03610
Langmuir 2024, 40, 4772−4778

power conversion efficiency; PTAA, poly[bis(4-phenyl)(2,4,6-trimethylphenyl]amine; PEDOT:PSS, poly(3,4-ethylenedioxythiophene):poly(styrenesulfonate); V_{OC}, open-circuit voltage; *FF*, fill factor; BHJ, bulk-heterojunction; ATR-FTIR, Fourier transform infrared spectroscopy; XPS, X-ray photoelectron spectroscopy; AFM, atomic force microscope; SEM, scanning electron microscope; EDS, energy dispersive spectroscopy; MD, molecular dynamic; HOMO, highest occupied molecular orbital; LUMO, lowest unoccupied molecular orbital; VBM, valence band maximum; PM6, poly[[4,8-bis[5-(2-ethylhexyl)-4-fluoro-2-thienyl]benzo[1,2-b:4,5-b′]dithiophene-2,6-diyl]-2,5-thiophenediyl[5,7-bis(2-ethylhexyl)-4,8-dioxo-4H,8H-benzo[1,2-c:4,5-c′]dithiophene-1,3-diyl]-2,5-thiophenediyl]; (Y6), 2,2′-[[12,13-Bis(2-ethylhexyl)-12,13-dihydro-3,9-diundecylbisthieno[2″,3″:4′,5′]thieno-[2′,3′:4,5] pyrrolo[3,2-e:2′,3′-g][2,1,3]benzothiadiazole-2,10-diyl]bis[methylidyne(5,6-difluoro-3-oxo-1H-indene-2,1(3H)-diylidene)]]bis[propanedinitrile]; ETL, electron transport layer; PSK, perovskite

REFERENCES

(1) Luo, D.; Yang, W.; Wang, Z.; Sadhanala, A.; Hu, Q.; Su, R.; Shivanna, R.; Trindade, G. F.; Watts, J. F.; Xu, Z.; Liu, T.; Chen, K.; Ye, F.; Wu, P.; Zhao, L.; Wu, J.; Tu, Y.; Zhang, Y.; Yang, X.; Zhang, W.; Friend, R. H.; Gong, Q.; Snaith, H. J.; Zhu, R. Enhanced Photovoltage for Inverted Planar Heterojunction Perovskite Solar Cells. *Science* **2018**, *360*, 1442−1446.

(2) Rajagopal, A.; Yao, K.; Jen, A. K. Y. Toward Perovskite Solar Cell Commercialization: A Perspective and Research Roadmap Based on Interfacial Engineering. *Adv. Mater.* **2018**, *30*, No. 1800455.

(3) Wu, X.; Li, B.; Zhu, Z.; Chueh, C.-C.; Jen, A. K. Y. Designs from Single Junctions, Heterojunctions to Multijunctions For High-Performance Perovskite Solar Cells. *Chem. Soc. Rev.* **2021**, *50*, 13090−13128.

(4) Wu, S.; Li, Z.; Li, M.-Q.; Diao, Y.; Lin, F.; Liu, T.; Zhang, J.; Tieu, P.; Gao, W.; Qi, F.; Pan, X.; Xu, Z.; Zhu, Z.; Jen, A. K. Y. 2D Metal−Organic Framework for Stable Perovskite Solar Cells With Minimized Lead Leakage. *Nat. Nanotechnol.* **2020**, *15*, 934−940.

(5) Li, X.; Hoffman, J. M.; Kanatzidis, M. G. The 2D Halide Perovskite Rulebook: How the Spacer Influences Everything from the Structure to Optoelectronic Device Efficiency. *Chem. Rev.* **2021**, *121*, 2230−2291.

(6) Wu, S.; Li, Z.; Zhang, J.; Wu, X.; Deng, X.; Liu, Y.; Zhou, J.; Zhi, C.; Yu, X.; Choy, W. C. H.; Zhu, Z.; Jen, A. K. Y. Low-Bandgap Organic Bulk-Heterojunction Enabled Efficient and Flexible Perovskite Solar Cells. *Adv. Mater.* **2021**, *33*, No. 2105539.

(7) Docampo, P.; Ball, J. M.; Darwich, M.; Eperon, G. E.; Snaith, H. J. Efficient Organometal Trihalide Perovskite Planar-Heterojunction Solar Cells on Flexible Polymer Substrates. *Nat. Commun.* **2013**, *4*, 2761.

(8) Xu, J.; Boyd, C. C.; Yu, Z. J.; Palmstrom, A. F.; Witter, D. J.; Larson, B. W.; France, R. M.; Werner, J.; Harvey, S. P.; Wolf, E. J.; Weigand, W.; Manzoor, S.; van Hest, M. F. A. M.; Berry, J. J.; Luther, J. M.; Holman, Z. C.; McGehee, M. D. Triple-Halide Wide−Band Gap Perovskites with Suppressed Phase Segregation For Efficient Tandems. *Science* **2020**, *367*, 1097−1104.

(9) Al-Ashouri, A.; Köhnen, E.; Li, B.; Magomedov, A.; Hempel, H.; Caprioglio, P.; Márquez, J. A.; Morales Vilches, A. B.; Kasparavicius, E.; Smith, J. A.; Phung, N.; Menzel, D.; Grischek, M.; Kegelmann, L.; Skroblin, D.; Gollwitzer, C.; Malinauskas, T.; Jošt, M.; Matič, G.; Rech, B.; Schlatmann, R.; Topič, M.; Korte, L.; Abate, A.; Stannowski, B.; Neher, D.; Stolterfoht, M.; Unold, T.; Getautis, V.; Albrecht, S. Monolithic Perovskite/silicon Tandem Solar Cell with > 29% Efficiency by Enhanced Hole Extraction. *Science* **2020**, *370*, 1300−1309.

(10) Yang, G.; Ni, Z.; Yu, Z. J.; Larson, B. W.; Yu, Z.; Chen, B.; Alasfour, A.; Xiao, X.; Luther, J. M.; Holman, Z. C.; Huang, J. Defect Engineering in Wide-bandgap Perovskites for Efficient Perovskite−Silicon Tandem Solar Cells. *Nat. Photonics* **2022**, *16*, 588−594.

(11) Li, F.; Jen, A. K.-Y. Interface Engineering in Solution-Processed Thin-Film Solar Cells. *Acc. Mater. Res.* **2022**, *3*, 272−282.

(12) Ullah, A.; Park, K. H.; Nguyen, H. D.; Siddique, Y.; Shah, S. F. A.; Tran, H.; Park, S.; Lee, S. I.; Lee, K.-K.; Han, C.-H.; Kim, K.; Ahn, S.; Jeong, I.; Park, Y. S.; Hong, S. Novel Phenothiazine-Based Self-Assembled Monolayer as a Hole Selective Contact for Highly Efficient and Stable p-i-n Perovskite Solar Cells. *Adv. Energy Mater.* **2022**, *12*, No. 2103175.

(13) Rombach, F. M.; Haque, S. A.; Macdonald, T. J. Lessons Learned from Spiro-OMeTAD and PTAA in Perovskite Solar Cells. *Energy Environ. Sci.* **2021**, *14*, 5161−5190.

(14) Bin, H.; Datta, K.; Wang, J.; van der Pol, T. P. A.; Li, J.; Wienk, M. M.; Janssen, R. A. J. Finetuning Hole-Extracting Monolayers for Efficient Organic Solar Cells. *ACS Appl. Mater. Interfaces* **2022**, *14*, 16497−16504.

(15) Lin, Y.; Adilbekova, B.; Firdaus, Y.; Yengel, E.; Faber, H.; Sajjad, M.; Zheng, X.; Yarali, E.; Seitkhan, A.; Bakr, O. M.; El-Labban, A.; Schwingenschlögl, U.; Tung, V.; McCulloch, I.; Laquai, F.; Anthopoulos, T. D. 17% Efficient Organic Solar Cells Based on Liquid Exfoliated WS2 as a Replacement for PEDOT:PSS. *Adv. Mater.* **2019**, *31*, No. 1902965.

(16) Zhang, G.; Lin, F. R.; Qi, F.; Heumüller, T.; Distler, A.; Egelhaaf, H.-J.; Li, N.; Chow, P. C. Y.; Brabec, C. J.; Jen, A. K. Y.; Yip, H.-L. Renewed Prospects for Organic Photovoltaics. *Chem. Rev.* **2022**, *122*, 14180−14274.

(17) Murugan, P.; Hu, T.; Hu, X.; Chen, Y. Advancements in Organic Small Molecule Hole-Transporting Materials for Perovskite Solar Cells: Past and Future. *J. Mater. Chem. A* **2022**, *10*, 5044−5081.

(18) Matsumoto, T.; Murakami, T.; Schlüter, F.; Murata, H.; Vohra, V.; Rizzo, F. Water-Soluble Organic Dyes as Efficient Anode Interlayer Materials for PEDOT:PSS-Free Inverted Bulk Heterojunction Solar Cells. *Sol. RRL* **2022**, *6*, No. 2100661.

(19) Jegorovė, A.; Momblona, C.; Daškevičienė, M.; Magomedov, A.; Degutyte, R.; Asiri, A. M.; Jankauskas, V.; Sutanto, A. A.; Kanda, H.; Brooks, K.; Klipfel, N.; Nazeeruddin, M. K.; Getautis, V. Molecular Engineering of Fluorene-Based Hole-Transporting Materials for Efficient Perovskite Solar Cells. *Sol. RRL* **2022**, *6*, No. 2100990.

(20) Li, M.; Xie, Y.; Lin, F. R.; Li, Z.; Yang, S.; Jen, A. K.-Y. Self-Assembled Monolayers as Emerging Hole-Selective Layers Enable High-Performance Thin-Film Solar Cells. *Innovation* **2023**, *4*, No. 100369.

(21) Li, E.; Bi, E.; Wu, Y.; Zhang, W.; Li, L.; Chen, H.; Han, L.; Tian, H.; Zhu, W.-H. Synergistic Coassembly of Highly Wettable and Uniform Hole-Extraction Monolayers for Scaling-up Perovskite Solar Cells. *Adv. Funct. Mater.* **2020**, *30*, No. 1909509.

(22) Abrusci, A.; Stranks, S. D.; Docampo, P.; Yip, H.-L.; Jen, A. K. Y.; Snaith, H. J. High-Performance Perovskite-Polymer Hybrid Solar Cells via Electronic Coupling with Fullerene Monolayers. *Nano Lett.* **2013**, *13*, 3124−3128.

(23) Lin, Y.; Firdaus, Y.; Isikgor, F. H.; Nugraha, M. I.; Yengel, E.; Harrison, G. T.; Hallani, R.; El-Labban, A.; Faber, H.; Ma, C.; Zheng, X.; Subbiah, A.; Howells, C. T.; Bakr, O. M.; McCulloch, I.; Wolf, S. D.; Tsetseris, L.; Anthopoulos, T. D. Self-Assembled Monolayer Enables Hole Transport Layer-Free Organic Solar Cells with 18% Efficiency and Improved Operational Stability. *ACS Energy Lett.* **2020**, *5*, 2935−2944.

(24) Nagata, M., Jr; Tsutsumi, N.; Kiyotsukuri, T. Synthesis and Properties of Polyamides Derived from Systematically Halogenated Terephthalic Acids with Fluorine, Chlorine, or Bromine Atoms. *J. Polym. Sci., Part A: Polym. Chem.* **1988**, *26* (1), 235.

(25) Metrangolo, P.; Canil, L.; Abate, A.; Terraneo, G.; Cavallo, G. Halogen Bonding in Perovskite Solar Cells: A New Tool for Improving Solar Energy Conversion. *Angew. Chem., Int. Ed.* **2022**, *61*, No. e202114793.

(26) Yao, H.; Ye, L.; Zhang, H.; Li, S.; Zhang, S.; Hou, J. Molecular Design of Benzodithiophene-Based Organic Photovoltaic Materials. *Chem. Rev.* **2016**, *116*, 7397−7457.

https://doi.org/10.1021/acs.langmuir.3c03610
Langmuir 2024, 40, 4772−4778

(27) Wang, Q.; Chueh, C.-C.; Zhao, T.; Cheng, J.; Eslamian, M.; Choy, W. C. H.; Jen, A. K.-Y. Effects of Self-Assembled Monolayer Modification of Nickel Oxide Nanoparticles Layer on the Performance and Application of Inverted Perovskite Solar Cells. *ChemSusChem* **2017**, *10*, 3794−3803.
(28) Yang, F.; Li, C.; Lai, W.; Zhang, A.; Huang, H.; Li, W. Halogenated Conjugated Molecules for Ambipolar Field-Effect Transistors and Non-Fullerene Organic Solar Cells. *Mater. Chem. Front.* **2017**, *1*, 1389−1395.
(29) Deng, X.; Qi, F.; Li, F.; Wu, S.; Lin, F. R.; Zhang, Z.; Guan, Z.; Yang, Z.; Lee, C.-S.; Jen, A. K.-Y. Co-assembled Monolayers as Hole-Selective Contact for High-Performance Inverted Perovskite Solar Cells with Optimized Recombination Loss and Long-Term Stability. *Angew. Chem., Int. Ed.* **2022**, *61*, No. 202203088.
(30) Wang, G.; Li, M.; Wei, Q.; Xiong, Y.; Li, J.; Li, Z.; Tang, J.; Wei, F.; Tu, H. Design of an AIE-Active Flexible Self-Assembled Monolayer Probe for Trace Nitroaromatic Compound Explosive Detection. *ACS Sens.* **2021**, *6*, 1849−1856.
(31) Chen, H.; Li, M.; Lu, Z.; Wang, X.; Yang, J.; Wang, Z.; Zhang, F.; Gu, C.; Zhang, W.; Sun, Y.; Sun, J.; Zhu, W.; Guo, X. Multistep Nucleation and Growth Mechanisms of Organic Crystals From Amorphous Solid States. *Nat. Commun.* **2019**, *10*, 3872.
(32) Magomedov, A.; Al-Ashouri, A.; Kasparavičius, E.; Strazdaite, S.; Niaura, G.; Jošt, M.; Malinauskas, T.; Albrecht, S.; Getautis, V. Self-Assembled Hole Transporting Monolayer for Highly Efficient Perovskite Solar Cells. *Adv. Energy Mater.* **2018**, *8*, No. 1801892.
(33) Al-Ashouri, A.; Magomedov, A.; Roß, M.; Jošt, M.; Talaikis, M.; Chistiakova, G.; Bertram, T.; Márquez, J. A.; Köhnen, E.; Kasparavičius, E.; Levcenco, S.; Gil-Escrig, L.; Hages, C. J.; Schlatmann, R.; Rech, B.; Malinauskas, T.; Unold, T.; Kaufmann, C. A.; Korte, L.; Niaura, G.; Getautis, V.; Albrecht, S. Conformal Monolayer Contacts with Lossless Interfaces for Perovskite Single Junction and Monolithic Tandem Solar Cells. *Energy Environ. Sci.* **2019**, *12*, 3356−3369.
(34) Chen, H.; Cheng, N.; Ma, W.; Li, M.; Hu, S.; Gu, L.; Meng, S.; Guo, X. Design of a Photoactive Hybrid Bilayer Dielectric for Flexible Nonvolatile Organic Memory Transistors. *ACS Nano* **2016**, *10*, 436−445.
(35) Li, M.; Xie, K.; Wang, G.; Zheng, J.; Cao, Y.; Cheng, X.; Li, Z.; Wei, F.; Tu, H.; Tang, J. An AIE-Active Ultrathin Polymeric Self-Assembled Monolayer Sensor for Trace Volatile Explosive Detection. *Macromol. Rapid Commun.* **2021**, *42*, No. 2100551.
(36) Jiang, W.; Li, F.; Li, M.; Qi, F.; Lin, F. R.; Jen, A. K. Y. π-Expanded Carbazoles as Hole-Selective Self-Assembled Monolayers for High-Performance Perovskite Solar Cells. *Angew. Chem., Int. Ed.* **2022**, *61* (51), No. 202213560.
(37) Lin, Y.; Zhang, Y.; Zhang, J.; Marcinskas, M.; Malinauskas, T.; Magomedov, A.; Nugraha, M. I.; Kaltsas, D.; Naphade, D. R.; Harrison, G. T.; El-Labban, A.; Barlow, S.; De Wolf, S.; Wang, E.; McCulloch, I.; Tsetseris, L.; Getautis, V.; Marder, S. R.; Anthopoulos, T. D. 18.9% Efficient Organic Solar Cells Based on n-Doped Bulk-Heterojunction and Halogen-Substituted Self-Assembled Monolayers as Hole Extracting Interlayers. *Adv. Energy Mater.* **2022**, *12*, No. 2202503.
(38) Laredo, T.; Leitch, J.; Chen, M.; Burgess, I. J.; Dutcher, J. R.; Lipkowski, J. Measurement of the Charge Number Per Adsorbed Molecule and Packing Densities of Self-Assembled Long-Chain Monolayers of Thiols. *Langmuir* **2007**, *23*, 6205−6211.
(39) Ghosh, M.; Yang, D.-S. Structures of self-assembled n-alkanethiols on gold by reflection high-energy electron diffraction. *Phys. Chem. Chem. Phys.* **2020**, *22*, 17325−17335.
(40) Liu, M.; Bi, L.; Jiang, W.; Zeng, Z.; Tsang, S.-W.; Lin, F. R.; Jen, A. K.-Y. Compact Hole-selective Self-assembled Monolayers Enabled by Disassembling Micelles in Solution for Efficient Perovskite Solar Cells. *Adv. Mater.* **2023**, *35*, No. e2304415.
(41) Zhao, B.; Gothe, B.; Groh, A.; Schmaltz, T.; Will, J.; Steinrück, H.-G.; Unruh, T.; Mecking, S.; Halik, M. Oligothiophene Phosphonic Acids for Self-Assembled Monolayer Field-Effect Transistors. *ACS Appl. Mater. Interfaces* **2021**, *13*, 32461−32466.
(42) Asyuda, A.; Gärtner, M.; Wan, X.; Burkhart, I.; Saßmannshausen, T.; Terfort, A.; Zharnikov, M. Self-Assembled Monolayers with Embedded Dipole Moments for Work Function Engineering of Oxide Substrates. *J. Phys. Chem. C* **2020**, *124*, 8775−8785.
(43) Oner, S. M.; Sezen, E.; Yordanli, M. S.; Karakoc, E.; Deger, C.; Yavuz, I. Surface Defect Formation and Passivation in Formamidinium Lead Triiodide (FAPbI3) Perovskite Solar Cell Absorbers. *J. Phys. Chem. Lett.* **2022**, *13*, 324−330.
(44) Chen, H.; Liu, T.; Zhou, P.; Li, S.; Ren, J.; He, H.; Wang, J.; Wang, N.; Guo, S. Efficient Bifacial Passivation with Crosslinked Thioctic Acid for High-Performance Methylammonium Lead Iodide Perovskite Solar Cells. *Adv. Mater.* **2020**, *32*, No. 1905661.
(45) Lv, J.; Tang, H.; Huang, J.; Yan, C.; Liu, K.; Yang, Q.; Hu, D.; Singh, R.; Lee, J.; Lu, S.; Li, G.; Kan, Z. Additive-Induced Miscibility Regulation and Hierarchical Morphology Enable 17.5% Binary Organic Solar Cells. *Energy Environ. Sci.* **2021**, *14*, 3044−3052.
(46) Yip, H.-L.; Hau, S. K.; Baek, N. S.; Ma, H.; Jen, A. K. Y. Polymer Solar Cells That Use Self-Assembled-Monolayer- Modified ZnO/Metals as Cathodes. *Adv. Mater.* **2008**, *20*, 2376−2382.
(47) Isikgor, F. H.; Zhumagali, S.; Merino, L. V. T.; De Bastiani, M.; McCulloch, I.; De Wolf, S. Molecular Engineering of Contact Interfaces for High-Performance Perovskite Solar Cells. *Nat. Rev. Mater.* **2022**, *8*, 89−108.
(48) Ullah, A.; Park, K. H.; Lee, Y.; Park, S.; Faheem, A. B.; Nguyen, H. D.; Siddique, Y.; Lee, K.-K.; Jo, Y.; Han, C.-H.; Ahn, S.; Jeong, I.; Cho, S.; Kim, B.; Park, Y. S.; Hong, S. Versatile Hole Selective Molecules Containing a Series of Heteroatoms as Self-Assembled Monolayers for Efficient p-i-n Perovskite and Organic Solar Cells. *Adv. Funct. Mater.* **2022**, *32*, No. 2208793.
(49) Li, X.; Zhang, W.; Guo, X.; Lu, C.; Wei, J.; Fang, J. Constructing Heterojunctions by Surface Sulfidation for Efficient Inverted Perovskite Solar Cells. *Science* **2022**, *375*, 434−437.

https://doi.org/10.1021/acs.langmuir.3c03610
Langmuir 2024, 40, 4772−4778